Journal of
Materials Chemistry C

PAPER

View Article Online
View Journal | View Issue

Cite this: *J. Mater. Chem. C*, 2022, **10**, 2639

Efficient charge generation and low open circuit voltage loss enable a PCE of 10.3% in small molecule donor and polymer acceptor organic solar cells†

Yi Li,[ab] Dan Deng, *[b] Rui Sun,[c] Sihua Wu,[b] LiLi Zhang,[b] Ziqi Zhang,[b] Jianqi Zhang,[b] Jie Min,[c] Guangjiu Zhao *[a] and Zhixiang Wei *[b]

Using a combination of polymer acceptors and small molecule donors (SM_D/P_A-type) is expected to exhibit easier morphology control because of the different diffusion speeds and solubilities due to their relatively large molecular weight difference, but lack of investigation. In this manuscript, we developed two novel small donor molecules **Se-1** and **Se-2**, with alkyl chains in the π-bridge near the donor core or far away from the donor core. We investigated their effects on the molecular properties, morphologies and device performances of the new type of OSCs. The alkyl chains away from the donor core (**Se-2**) exhibit ordered molecular packing ability, longer exciton lifetime, and an induced face-on packing mode in the blend. Consequently, the **Se-2**/polymer acceptor blend, with a concurrently high charge generation and low open-circuit voltage loss, reached a best PCE of 10.3%, which is higher than that of the **Se-1/**polymer acceptor (9.4%). The result shows the highest PCE in the less investigated SM_D/P_A-type OSCs. Through comparison of other types of OSCs based on the two small donor materials, we find that the small molecules and PJ1 exhibited high miscibility, and we emphasize the importance of enhancing the Flory–Huggins interaction parameter and molecular crystallinity in further photovoltaic material design in SM_D/P_A-type OSCs.

Received 16th September 2021,
Accepted 2nd November 2021

DOI: 10.1039/d1tc04428a

rsc.li/materials-c

Introduction

Organic solar cells (OSCs) based on polymer acceptors attract considerable attention for potential commercial application because of their superior thermal and light stability, and excellent efficiency.[1–11] The energy loss for the polymer acceptor could also be as low as 0.47 eV.[6,8] Importantly, the polymer acceptor could be easily polymerized from the small acceptors, and their opto-electrical properties could be well tuned through the monomer or ternary copolymerization.[2,3,12–14] Consequently, the power conversion efficiency (PCE) has surpassed 16% for the binary all-polymer OSCs and reached 17% for ternary all-polymer OSCs.[11,15] Adopting all the merits of polymer acceptors, however, the OSCs using the combination of polymer acceptors and small molecule donors (SM_D/P_A-type) have attracted less attention than other systems.[16,17] In 2019, Wang *et al.* exhibited excellent thermal stability of SM_D/P_A-type OSCs.[16] A PCE of 8.1% was obtained by utilizing the B ← N containing polymer PBN-11 as the acceptor and a small molecule DR3TBDTC as the donor. After thermal annealing the active layer at 180 °C for 7 days, the DR3TBDTC: PBN-11 based OSC maintained 89% of the initial PCE. Furthermore, they optimized the polymer structure to PBN-15. Using BD3T as a donor, the PCE was optimized to 9.5%.[17] It is noteworthy that the OSC retained excellent thermal stability. However, the PCE of SMD/PA-type OSCs is lagging far behind that of other systems, due to the poor absorption spectrum of polymer acceptor of PBN system as well as their poorly explored morphology.

In all types of OSCs, the morphology is a fatal factor to decide the performance of the devices, as the morphology determines the lifetime and the distribution of all of the intermediate states (such as exciton, charge transfer states and hole/electron), and their probable process (such as charge transfer, energy transfer and hybridization) between a photon and an electron in a circuit loop, which are directly related to the PCE.[18–21] Different types of OSCs have their own morphology features.[22–24] Consequently, they differed from other vastly investigated types of OSCs, including polymer OSCs (polymer

---

[a] *Department of Chemistry, Molecular Dynamic Chemistry Center, Tianjin Key Laboratory of Molecular Optoelectronic Sciences, School of Science, Tianjin University, Tianjin 300354, China*
[b] *National Center for Nanoscience and Technology, Beijing 100190, China*
[c] *The Institute for Advanced Studies, Wuhan University, Wuhan 430072, China*

† Electronic supplementary information (ESI) available. See DOI: 10.1039/d1tc04428a

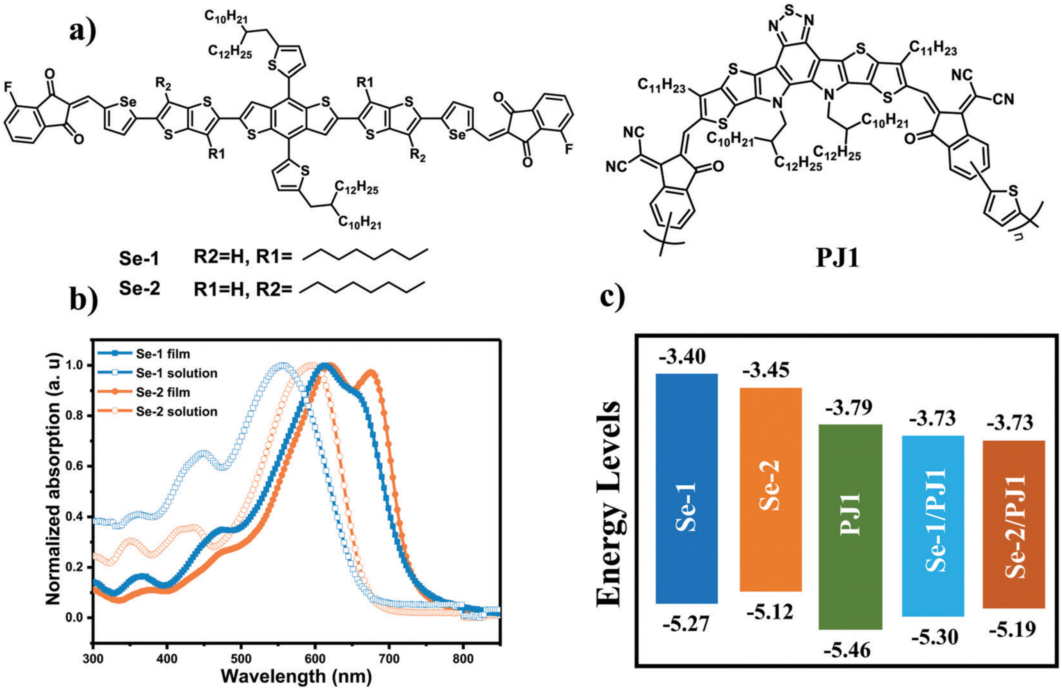

Fig. 1 Molecule properties: (a) molecule structures of donors and polymer acceptors; (b) absorption spectrum of small molecules; (c) energy level alignment of small molecules and polymer acceptor in pristine and blend film.

donor + small acceptor), all-small-molecule OSCs (small donor + small acceptor), and all-polymer OSCs (polymer donor + polymer acceptor). The SM_D/P_A-type contains a highly crystalline small donor and polymer acceptor. Hence, the morphology should be quite different from the previous ones, which is of significance to be investigated. Learning from the experience of other types of OSCs, adjusting the alkyl chains is a simple, but effective approach to tune the morphology.[23,25–28]

Hence, in this manuscript, two novel small donors, named **Se-1** and **Se-2** (Fig. 1a), were developed and the two small molecules differed in the positions of alkyl chains attached to the π-bridge. The small molecule with the alkyl chains near the donor core is **Se-1**, and the one with the chains away from the donor core is **Se-2**. By having the alkyl chain position shifted away from the donor core together, the molecular crystallinity was well tuned, and the average donor exciton lifetime was increased from 128 to 150 ps. Using a much more red-shifted PJ1 (*ca.* 160 nm red-shifted than the reported B ← N containing polymers) as the polymer acceptor, the packing mode of the donors with **Se-2** was induced to the preferential face-on packing mode, while **Se-1** retained the edge-on packing mode. For the concurrently more efficient charge generation and low voltage loss, the device based on **Se-2** exhibits a higher power conversion efficiency (PCE) of 10.3%, with simultaneously higher J_{sc} and V_{oc}. By comparison with other types of OSCs based on the two small donor materials, we found that the small molecules and PJ1 exhibited superior miscibility, indicating that the high crystallinity material **Se-2** won the better PCE in this SM_D/P_A-type OSCs. The miscibility of this type is better than that of the ASM-OSCs type OSC, but also may lead to smaller phase separation, which may be more difficult to form an interpenetrating network structure. To further improve the PCE in SMD/PA-type OSCs, we emphasize the importance of enhancing the Flory–Huggins interaction parameter rather than miscibility in further photovoltaic material design.

Results and discussions

Synthesis and molecular structure

The synthesized route of the two donor materials is shown in Scheme S1 (ESI†), and the detailed synthetic procedures and structure characterizations are shown in the ESI.† The molecular backbone of the two molecules originated from our previous work,[27,29] which exhibited good planarity and high hole mobility. The incorporation of Se in the π-bridge is to enhance the molecular interaction through d-orbitals. The choice of the end-capped acceptor is an overall consideration of energy level and planarity of aromatic end-capped acceptor. In all of our previous work, the alkyl chains were close to the TBDT core, which would disturb the molecular planarity. Consequently, in this work, we shifted the alkyl chains away from the TBDT core to investigate the alkyl chains position effect on the molecular properties, morphologies and the SM_D/P_A-type device performances. As expected, compared to **Se-1**, shifting the alkyl chains away from the donor core led to a decreased torsion between the donor core and the π-bridge, and the torsion angle for **Se-2** decreased *ca.* 15° (Fig. S1, ESI†), indicating its better backbone planarity. It should be mentioned that the two molecules exhibited good solubility in common organic solvents, benefiting the fabrication of solution-processable photovoltaic devices.

Optical and electrochemical properties

The ultraviolet (UV)-visible absorption spectra of the two small donors and polymer acceptor in chloroform solution and thin films are shown in Fig. 1b. Out of our expectation, the alkyl chains in the two different positions make a big difference on the absorption spectrum whether in the solution or the film. As compared to **Se-1**, **Se-2** with alkyl chains away from the donor core red-shifted *ca.* 40 nm in the solution, which should be due to the longer effective conjugated length resulting from less torsional angle. Simultaneously, in the film, the ratio of its shoulder peak to internal charge transfer peak (ICT) is 0.983, which is obviously stronger than that of **Se-1** (0.887). Furthermore, the absorption spectrum edge is much sharper. These phenomena indicate that **Se-2** exhibits ordered and stronger molecular packing, which could be due to its more planar molecular backbone as discussed above. The film absorption onsets of the two molecules are 730 and 736 nm, corresponding to the medium bandgaps of 1.70 and 1.68 eV, respectively. As for the polymer acceptor PJ1,[13] it shows excellent absorption in the range of 600 to 870 nm with a maximum absorption peak at 792 nm in the film. Consequently, the absorption spectra of the two small donors and the polymer acceptor are complemented well.

The HOMO energy level and the lowest occupied molecular orbital (LUMO) energy levels of the molecules in the pristine films were measured by electrochemical cyclic voltammetry (CV), and the calculated equation is: $E_{\mathrm{HOMO/LUMO}} = -\mathrm{e}\,[E_{\mathrm{ox/red}} - E_{1/2}(\mathrm{Fc/Fc^+}) + 4.8]$ (eV). The HOMO energy levels for **Se-1** and **Se-2** are −5.27 and −5.12 eV, respectively, and the corresponding LUMO energy levels are −3.40 and −3.44 eV, respectively (as shown in Fig. 1c and Fig. S2a, ESI†). The results demonstrate that moving the alkyl chains away from the donor core upshifted the HOMO energy level. The upshifted HOMO energy level of **Se-2**, compared to **Se-1**, should be due to its longer effective and planar conjugated backbone. It should be mentioned that the tendency of the HOMO energy levels measured by CV for **Se-1** and **Se-2** is the same with calculation by DFT method (Fig. S3 and Table S1, ESI†). As compared to PJ1 (the HOMO and LUMO energy level is −5.46 and −3.78 eV), the two small molecules exhibit medium driving force (*ca.* 0.3 eV) for both hole/electron transfers.

The energy levels in the blend film are always different from those in the pristine film because of their different band-bending, dipole and aggregation induced by the second component. Consequently, the energy levels of the blend films were also measured by CV measurements (Fig S2b, ESI†). The HOMO energy levels for **Se-1** and **Se-2** were −5.30 and −5.19 eV, and the corresponding LUMO energy levels were the same with a value of −3.73 eV, respectively. As compared to pristine films, both the HOMO energy levels are downshifted, especially for the **Se-2** with a downshifted value of 0.07 eV, which is larger than that of **Se-1** (0.03 eV). However, the HOMO energy level for **Se-1** is still lower than that of **Se-2**. The blending of PJ1 does not change their variation trend in the pristine films. From the above results and analysis, both donor molecules display matched energy levels with the polymer acceptor, with different and moderate driving forces for hole transfer.

Photovoltaic properties of OSC devices

To investigate the device performances of the two small molecules with the polymer acceptor, a configuration of indium–tin–oxide(ITO)/poly(3,4-ethylenedioxy-thiophene): polystyrene sulfonate (PEDOT: PSS)/active layer/Poly(9,9-bis(3′-(*N*,*N*-dimethyl)-*N*-ethylammoinium-propyl-2,7-fluorene)-*alt*-2,7-(9,9-dioctylfluoren-e)) dibromide (PFNBr)/Ag was chosen to fabricate the devices, and the device performance was tested under AM 1.5 solar illumination. Fig. 2a and b show the current density–voltage (*J*–*V*) curves of the best device performances and their corresponding external quantum efficiency (EQE), and Table 1 summarizes the detailed best and averaged parameters. The best devices for the two small molecules were fabricated at a D:A ratio of 1.75 : 1. Thereinto, **Se-2** utilized 1% chloronaphthalene (CN) as an additive with thermal annealing (TA) for 10 minutes, while **Se-1** utilized 1% 2-chlorophenol (CP) as an additive without TA, and all of the detailed device optimization data are displayed in Tables S2 and S3 (ESI†). As shown in Table 1, under optimal conditions, the device based on **Se-2**: PJ1 blend obtained an outstanding PCE of 10.3% with a V_{oc} of 0.87 V, a J_{sc} of 19.4 mA cm^{-2}, and an fill factor (FF) of 61.2%. The PCE of **Se-1**: PJ1 device is in hot pursuit of the **Se-2**: PJ1 with a PCE of 9.4% with a V_{oc} of 0.84 V, J_{sc} of 18.5 mA cm^{-2}, and fill factor (FF) of 59.9%. Compared to **Se-1**, all of the parameters for **Se-2** are higher, even for V_{oc}, although the HOMO energy level of **Se-2** upshifted *ca.* 0.11 eV whether in the pristine film or blend film. This abnormal phenomenon will be analysed in the following text. As shown in Fig. 2b and Table 1, the different J_{sc} of the two devices contribute the main disparity of their photovoltaic performances. The external quantum efficiency (EQE) curves of all devices based on the two small molecules exhibit relatively similar and square shapes, and the maximum value of EQE for **Se-1** and **Se-2** are 67% and 72%, respectively. The different J_{sc} and EQE should be partly due to their diverse photon utilization efficiency as deduced from the EQE values in the PJ1 absorption region. It is noteworthy that the FF is consistent with the trend of J_{sc}, both of which would be analysed in detail in the following parts. To uncover the loss of the J_{sc} and FF, the photocurrent density (J_{ph}) *versus* effective voltage (V_{eff}) was tested as shown in Fig. 2c (J_{ph} is given by $J_{\mathrm{ph}} = J_{\mathrm{L}} - J_{\mathrm{D}}$, where J_{L} and J_{D} are the current densities under illumination and in the dark, respectively. $V_{\mathrm{eff}} = V_0 - V_{\mathrm{app}}$, where V_0 is the voltage at which $J_{\mathrm{ph}} = 0$, and V_{app} is the external voltage). The saturated J_{ph} ($J_{\mathrm{ph,sat}}$) represents the J_{ph} at higher V_{eff} ($V_{\mathrm{eff}} > 2$), where all the excitons are dissociated and collected. Consequently, the ratios of $J_{\mathrm{ph}}/J_{\mathrm{ph,sat}}$ can be used to judge the overall efficiency of exciton dissociation and charge collection. Under short-circuit condition, the ratios of $J_{\mathrm{ph}}/J_{\mathrm{ph,sat}}$ were 0.93 and 0.95 for **Se-1**/PJ1 and **Se-2**/PJ1, respectively. The higher value of $J_{\mathrm{sc}}/J_{\mathrm{ph,sat}}$ for **Se-2**/PJ1 indicates its slightly more efficient exciton dissociation efficiency, which we will further discuss in the charge generation part. Under lower effective

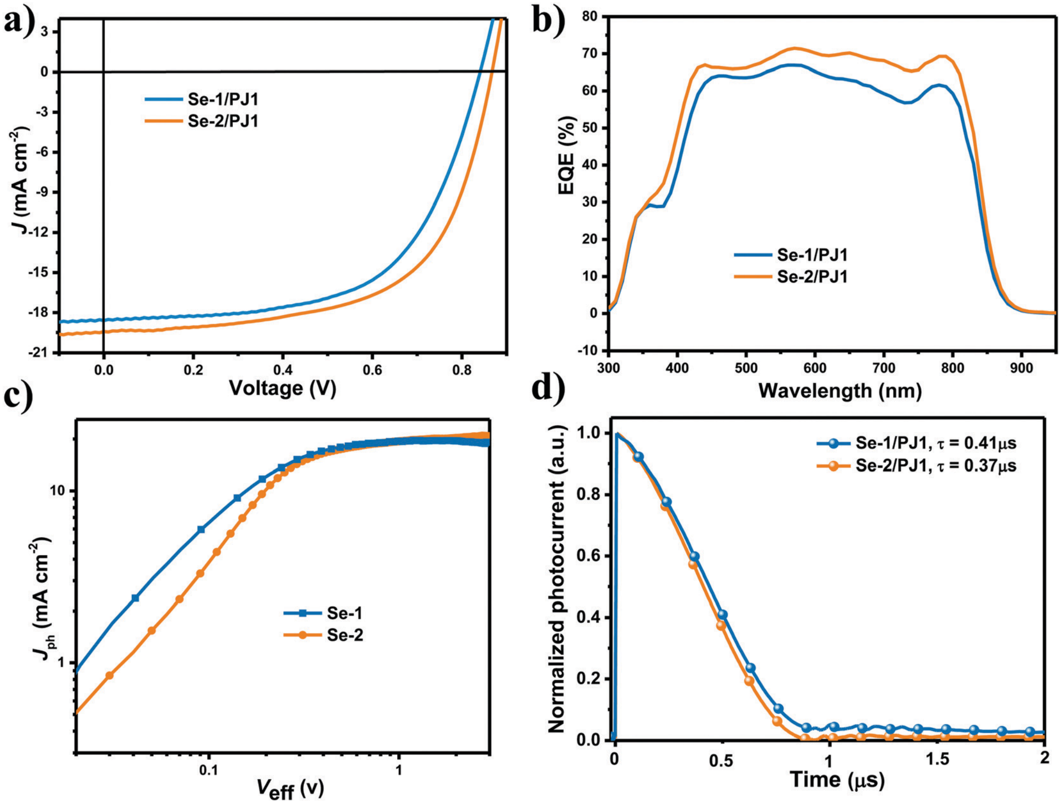

Fig. 2 Device performances. (a) J–V curves; (b) corresponding EQE curves based on image a; (c) V_{eff}–J_{ph} curves for the two devices; (d) TPC curves of the devices based on the two small molecules.

Table 1 Device performances based on the device structure of the ITO/PEDOT:PSS/active layer/PFNBr/Ag

Donor	V_{oc} (V)	J_{sc} (mA cm^{-2})	FF (%)	PCE(%)	$J_{\mathrm{sc\ cal}}$
Se-1	0.84 (0.84 ± 0.02)	18.60 (18.42 ± 0.40)	59.9 (58.7 ± 1.0)	9.4 (9.1 ± 0.2)	18.00
Se-2	0.87 (0.87 ± 0.01)	19.42 (19.34 ± 0.17)	61.2 (59.8 ± 0.8)	10.3 (10.1 ± 0.2)	19.19

The averaged PCE were obtained by 10 devices.

reverse voltage (V_{eff} = 0.4 V), the ratios of $J_{\mathrm{ph}}/J_{\mathrm{ph,sat}}$ for **Se-1** and **Se-2** were 0.77 and 0.79, respectively. The higher $J_{\mathrm{ph}}/J_{\mathrm{ph,sat}}$ for **Se-2**/PJ1 suggests its more efficient charge collection efficiency. The higher charge collection for **Se-2**/PJ1 could be further convinced by its faster charge extraction speed measured by transient photocurrent (Fig. 2d, the charge extraction for **Se-2**/PJ1 and **Se-1**/PJ1 is 0.41 and 0.37 μs, respectively). Their equal linear slope value (close to 1) for log function of J_{sc} to light intensity (Fig. S4, ESI†) inferred that both devices exhibited effective suppressed bimolecular recombination. The previous phenomena indicate that the **Se-2**/PJ1 devices have a slightly more efficient charge generation and higher charge collection. Consequently, the efficient charge generation and higher charge collection should be the main reason for the efficient utilization of photons and fill factor.

Molecular packing and morphology

Grazing incidence wide-angle X-ray scattering (GIWAXS) was used to investigate the molecular crystallinity of the two small molecules and their blend microstructure with the polymer acceptor. The 2-dimensional images and 1-dimensional profiles based on their pristine films and blends under optimized condition are displayed in Fig. 3a and c, and all of the detailed data of the GIWAXS has been summarized in Table S4 (ESI†). As shown in Fig. 3a, both molecules exhibit good crystallinity and adopt a preferential edge on the molecular packing mode due to the obvious lamellar (n00; n = 1, 2, 3) peaks in the out-of-plane (OOP) direction and the (010) peak in the in-plane (IP) direction. The π–π stacking distance for the two pristine films are nearly the same with a value of 3.54 Å. However, in comparison with **Se-1**, **Se-2** exhibits stronger molecular packing ability for the following three reasons: (1) its emergency of the lamellar (400) peak in the OOP direction; (2) its longer crystal coherence lengths (CCLs) in the OOP π–π stacking direction (lengthened from 40.92 to 48.65 Å); (3) its longer CCLs in the IP alkyl chains stacking direction (lengthened from 44.20 to 174.78 Å). The better molecular packing ability of **Se-2** should be due to its better molecular planarity, as discussed above.

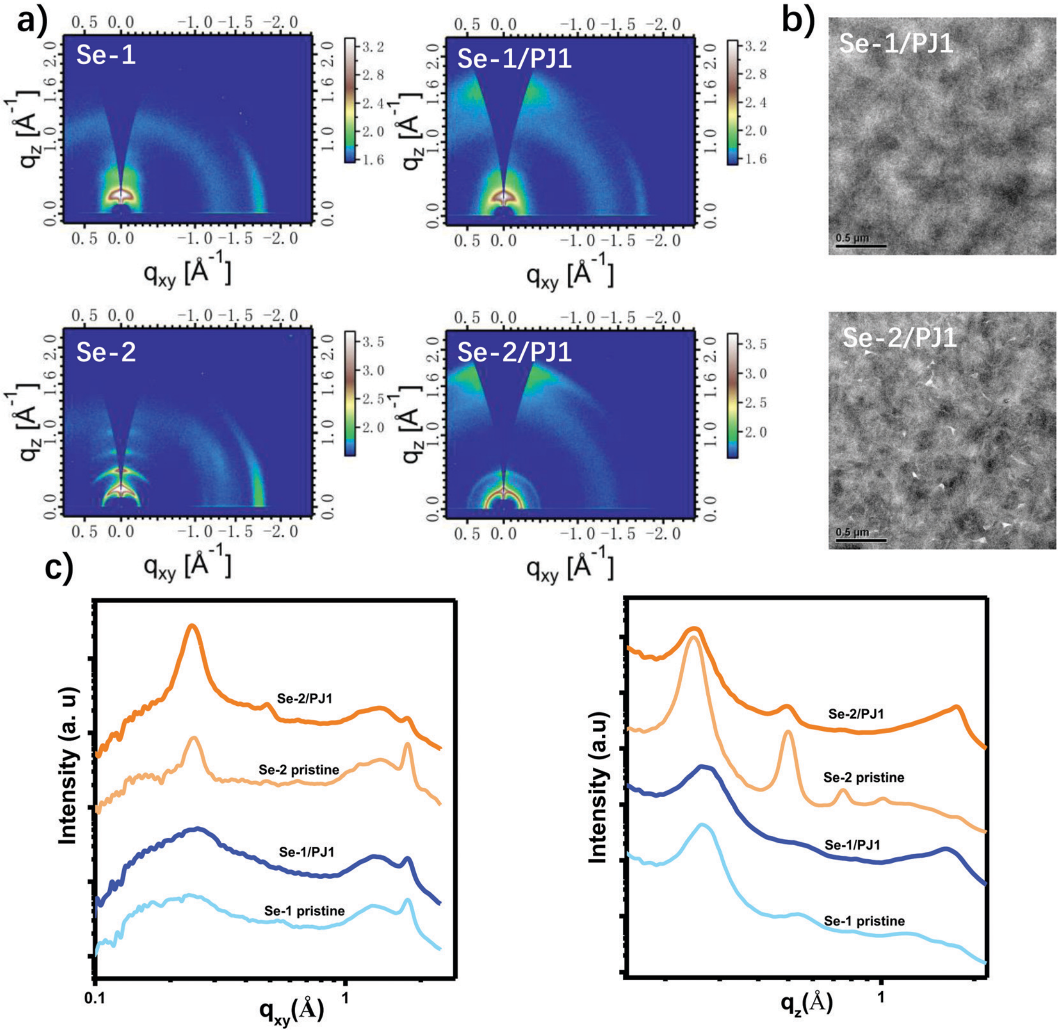

Fig. 3 (a) 2-D GIWAXS images based on the pristine films and optimized blend films; (b) TEM images for the optimized blend; (c) 1-D GIWAXS curves corresponding to Fig. (a).

After adding the polymer acceptor and additives, **Se-1** retained its edge-on packing as deduced from the (010) peak in the IP direction. However, for **Se-2**, an obvious (010) peak has emerged in the OOP direction besides the (010) peak of the polymer acceptor, and the (010) peak of the IP direction has disappeared, illustrating that the molecular packing has been induced by the polymer acceptor (the GIWAXS of pristine films with additives did not change the packing mode, Fig. S5, ESI†). Consequently, in the optimized blends, **Se-2** exhibits a hybrid face-on/edge-on packing mode. The CCL for (010) in the IP direction for the **Se-1**/PJ1 blend is 30.1 Å, which is slightly higher than that of the **Se-2**/PJ1 blend (28.2 Å). However, **Se-2**/PJ1 has an extra ordered π–π stacking in the OOP direction with a CCL of 48.2 Å. The above results demonstrated that **Se-2**/PJ1 exhibited much more ordered packing than the **Se-1**/PJ1 blend, which would benefit the charge transport. However, there is no obvious PJ1 lamella peak in either **Se-1**/PJ1 and **Se-2**/PJ1 blend, perhaps due to its weak crystallinity after blending with small molecules or its lamella peak is buried in that of the donor materials.

Transmission electronic microscopy (TEM) was used to further confirm the bulk phase separation (Fig. 3c). As compared to the **Se-1**/PJ1 blends, the **Se-2**/PJ1 blends display more obvious fibrous structures, implying its better interpenetrating network and higher crystallinity, which should be beneficial for charge generation and charge collection. As shown in the atomic force microscopy (AFM) height images in Fig. S6 (ESI†), the root-mean-square (RMS) values of the surface roughness for both **Se-1**/PJ1 and **Se-2**/PJ1 blends are relatively large, which is consistent with their good crystallinity. The higher RMS value of **Se-2**/PJ1 (R_q = 4.9) than that of **Se-1**/PJ1 (R_q = 3.9) further confirms the better crystallinity of **Se-2** in the blend.

Morphology impact on charge transport

To determine the impact of morphology on the routes and barriers of charge transport, which was fatal to the FF and J_{sc}, the hole and electron mobility of the small molecules in the pristine and blends were measured using the space-charge limited current (SCLC) method by utilizing hole-only and electron-only device structures, and the detailed data are shown

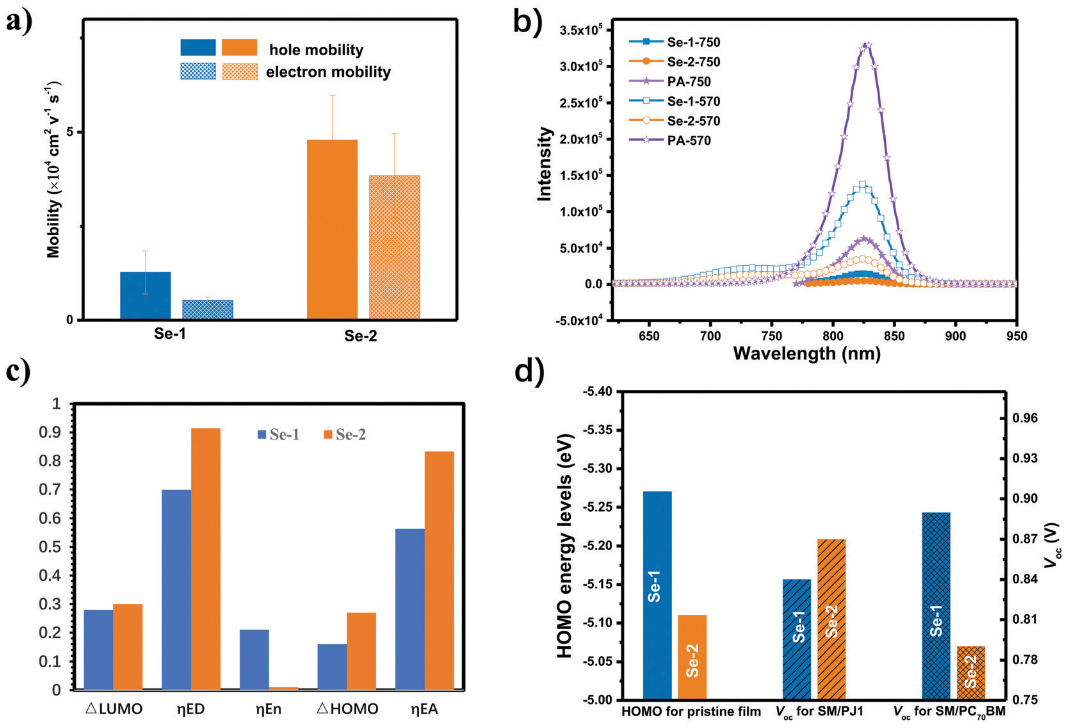

Fig. 4 The effects of different morphologies on different aspects: (a) hole/electron mobility based on the optimized blend; (b) PL spectra based on the optimized blend and the PJ1 pristine film at the excitation wavelengths of 570 nm and 750 nm; (c) detailed parameters for the charge generation based on the fitting from the PL spectra; (d) HOMO energy levels and their V_{oc} based on the small molecules/PJ1 devices and small molecules/$PC_{70}BM$ blends.

in Fig. 4a. The two small molecules in the pristine films exhibit high hole mobility ($>7.35 \times 10^{-4}$ cm^2 V^{-1} S^{-1}) with increased crystallinity, and the averaged hole mobility increased from 7.35×10^{-4} to 9.24×10^{-4} cm^2 V^{-1} S^{-1}. After PJ1 addition, the averaged hole mobility for **Se-2**/PJ1 is 4.79×10^{-4} cm^2 V^{-1} S^{-1}, which is much higher than that of **Se-1**/PJ1 (1.27×10^{-4} cm^2 V^{-1} S^{-1}). This is in positive correlation with their packing order. The averaged electron mobility is 5.25×10^{-5} and 3.81×10^{-4} cm^2 V^{-1} S^{-1} for **Se-1** and **Se-2**, respectively. The **Se-2** achieved a mobility that was almost one order magnitude higher than that of **Se-1**, which should be due to its electrical connectivity between the PJ1 domains in the blend films resulting from its fiber interpenetrating network (as shown in TEM image, Fig. 3c). The higher hole/electron mobility and balanced hole/electron transport should be the reason for the improved FF and charge collection in the **Se-2**/PJ1 blend.

Morphology impact on charge generation

As analysed in the photophysical process, **Se-2**/PJ1 presented a more efficient charge generation. Consequently, the steady state photoluminescence (PL) measurement was applied to evaluate the efficiency of the charge generation.

First, the steady-state PL spectrum and time-resolved photoluminescence (TRPL) were obtained for the small donors and acceptors. Both donors and PJ1 exhibited medium strong PL intensity, which was quite beneficial for exciton quenching analysis. The TRPL results demonstrate that the averaged exciton lifetime for **Se-2** is 150 ps, which is higher than that of **Se-1** (128 ps, Fig. S7 and Table S5, ESI†). This result correlates well with the better crystallinity of **Se-2**. The steady-state PL spectrum of the blends was measured to investigate the quenching efficiency of the donor and acceptor excitons to evaluate the charge generation efficiency (Fig. 4b and Fig. S8, ESI†). At the excitation wavelength of 750 nm, an obvious PL peak was found in *ca.* 826 nm for both blends, which was attributed to the PL spectrum of the acceptor. The calculated quenching efficiency of the PJ1 excitons is 58.0% for **Se-1** and 86.5% for **Se-2**. This result suggests that PJ1 has not been completely quenched by the two small molecules, and PJ1 exhibits more efficient hole transfer in the **Se-2**/PJ1 blend than the **Se-1**/PJ1 blend, which should be due to its higher driving force and faster extraction of the holes.[30] This result further confirms its efficient charge generation in the **Se-2**/PJ1 blend. It should be mentioned that for **Se-1**, the efficiency of the hole transfer is below the EQE, indicating that there is some other charge generation process such as hybridization for their smaller ΔHOMO.[31]

At the excitation wavelength of 560 nm, the quenching efficiencies for **Se-1** and **Se-2** are nearly equal (*ca.* 90%), which is slightly contrary with its higher EQE of **Se-2**/PJ1, as deduced by the residual PL peak intensity of the donor in the range of 650–750 nm. Due to the PL spectrum of the donor and the absorption spectrum of the acceptor severely overlapping (Fig. S9, ESI†), we speculate that there is a fraction of the Foerster energy transfer (FRET) from the donor to acceptor, which acts as a competition pathway for the donor exciton loss when the hole transfer is inefficient.[21,23] In order to evaluate the efficiency of the electron transfer of the small molecules ($\eta_{\mathrm{EH,D}}$) and the fraction of undissociated excitons undergoing FRET (η_{Entr}), the blend PL spectrum can be estimated by fitting to the PL signal of the blend film with the two following equations, according to the literature:[32,33]

$$\mathrm{PL}_{\mathrm{blend}}(\lambda) = (1 - \eta_{\mathrm{EH,D}} - \eta_{\mathrm{Entr}})f_{\mathrm{D}}\mathrm{PL}_{\mathrm{D}}(\lambda) + [\eta_{\mathrm{Entr}}f_{\mathrm{D}} + (1 - \eta_{\mathrm{EH,D}})f_{\mathrm{A}}]\mathrm{PL}_{\mathrm{A}}(\lambda)$$

$$f_{\mathrm{D/A}}(\lambda) = x_{\mathrm{D/A}}k_{\mathrm{D/A}}(\lambda)[x_{\mathrm{D}}k_{\mathrm{D}}(\lambda) + x_{\mathrm{A}}k_{\mathrm{A}}(\lambda)]$$

where f(λ) is the absorption fraction in either the donor or acceptor, PL(λ) is the PL spectrum, x is the volume fraction, and k is the absorption coefficient. The fitting results have been summarized in Fig. 4c and Table S6 (ESI†), and the fitting details are shown in Fig. S10 (ESI†). The fitted quenched efficiency and the tendency for the two acceptor excitons (η_{EA}) are approximate to the measurements, as discussed above (the excitation wavelength of 750 nm). Thereinto, the fitted energy transfer efficiency (η_{ENTR}) for **Se-1** is 21%. Meanwhile, for **Se-2**, the fitted energy transfer efficiency is almost 0% (the corresponding charge transfer efficiency is 69.9% and 91.4% for **Se-1** and **Se-2**, respectively). The higher efficiency of the charge transfer and lower FRET for the **Se-2**/PJ1 blend should be mainly due to the faster electron extraction ability owing to its higher electron mobility and fiber interpenetrating morphology.

From the above analysis, beside the driving force, the higher hole/electron mobility resulting from the order packing and fiber interpenetrating morphology suppressed the energy transfer and facilitated charge generation in the **Se-2**/PJ1 blend, leading to an improved J_{sc}.

Morphology impact on the V_{oc} loss.

For the contradictory results between the HOMO energy levels (pristine film or blend film) and the V_{oc}, we turned to the small molecules/$\mathrm{PC_{70}BM}$ type device to see their V_{oc} variation. The devices based on **Se-1**/$\mathrm{PC_{70}BM}$ and **Se-2**/$\mathrm{PC_{70}BM}$ were fabricated and optimized, and the best device parameters are shown in Table S7 (ESI†). To our surprise, in the fullerene system, **Se-1**/$\mathrm{PC_{70}BM}$ exhibited much better device performance with a PCE of 8.96%, an FF of 75% and a V_{oc} of 0.89 V, which is much higher than that of **Se-2**/$\mathrm{PC_{70}BM}$ (PCE of 5.31% with a V_{oc} of 0.79 V and FF of 59.5%). As shown in Fig. 4d, the V_{oc} variation is consistent with their changed HOMO energy level. Consequently, the disparity between the tendency of V_{oc} and the HOMO energy level in the two different OSCs types, and the low V_{oc} loss in **Se-2**/PJ1 should be due to its unique blend morphology.

Actually, the morphology of the active layer is quite important to V_{oc}.[19,20] As investigated by the Nguyen group, the devices that are based on the interface with the donor molecules face-on to the acceptor have a higher charge transfer state energy and less non-radiative recombination.[20] Consequently, the V_{oc} with face-on interface orientation is 0.15 V higher than the edge-on interface orientation. In our fullerene system, both **Se-1**/$\mathrm{PC_{70}BM}$ and **Se-2**/$\mathrm{PC_{70}BM}$ adopted edge-on packing mode. Its V_{oc} variation is consistent with their change of the HOMO energy levels. As in the PJ1 system, **Se-2** was induced to the face-on molecular packing mode by PJ1, and this induction may happen at the donor/acceptor interface.[34] However, **Se-1** retained the edge-on molecular packing. Probably, the face-on interface orientation and packing mode should be the reason for the low V_{oc} loss for the **Se-2**/PJ1 device.

Flory–Huggins interaction parameter and comparison of different types of OSCs

As initiated by the large device performance difference in the fullerene systems and PJ1 systems based on the two small molecules, in this part, we investigate the morphology features of the $\mathrm{SM_D/P_A}$-type OSCs. Because the surface energy and Flory–Huggins interaction parameter (χ) are decisive to the phase separation and morphology formation, the contact angles were measured (Fig. S11, ESI†) and the detailed parameters are summarized in Table 2. **Se-1** exhibited a slightly higher surface tension with a value of 30.45 mN m^{-1} than that of **Se-2** (29.02 mN m^{-1}). Consequently, **Se-2**/PJ1 showed a slightly higher χ value of 0.05 than that of **Se-1**/PJ1 (0.01). It is noteworthy that both values are quite low, and the low values of the χ demonstrate better miscibility between the two molecules and PJ1 compared with other OSC systems.

To further certify this unique property of the $\mathrm{SM_D/P_A}$-type OSCs, the χ value for the small molecule/Y6 and small molecule/$\mathrm{PC_{70}BM}$ were also measured and calculated, and the detailed results are summarized in Table 2. The χ value for **Se-2**/Y6 is 0.31 and the χ value for **Se-2**/$\mathrm{PC_{70}BM}$ is 0.5, both of which are much higher than that of $\mathrm{SM_D/P_A}$-type OSCs. As for **Se-1**, the χ value for **Se-1**/Y6 is 0.18 and the χ value for **Se-2**/$\mathrm{PC_{70}BM}$ is 0.33. Consequently, compared to other types of OSCs, enhancing the crystallinity and domain purity rather than miscibility would be an effective strategy to further improve the PCE. The miscibility study also revealed the reason of the improved PCE for **Se-2**/PJ1 in this polymer acceptor system.

Due to the reported excellent thermal stability in the MA/PD-type OSCs,[15,16] we also tested the thermal stability of the **Se-2**/PJ1 and **Se-1**/PJ1 devices. After annealing for a half hour at 150 °C, the PCE of **Se-2**/PJ1 sustained 70%, while the PCE of **Se-1**/PJ1 decreased to 30% (Fig. S12, ESI†), indicating the better thermal stability of the **Se-2**/PJ1 device. It is noteworthy that the results also indicate that the higher value of the Flory–Huggins parameters lead to a more stable device, which is possibly because the morphology based on the optimized condition is much closer to its thermal-stable state.

Table 2 Surface tension and calculated Flory–Huggins interaction parameter

Materials	**Se-1**	**Se-2**	$\mathrm{PC_{70}BM}$	Y6	PJ1
γ [mN m^{-1}]	30.5	29.0	37.1	35.3	31.4
χ (**Se-1**)	—	—	0.33	0.18	0.01
χ (**Se-2**)	—	—	0.5	0.31	0.05

Conclusions

In summary, two novel small donor molecules were developed, with alkyl chains close to the donor core (**Se-1**) or far away from the donor core (**Se-2**). Both molecules exhibited complementary absorption spectra with the polymer acceptor PJ1. Shifting the alkyl chains away from the donor core (**Se-2**) led to better molecular planarity, higher HOMO energy level, and ordered molecular packing. After blending with the polymer acceptor PJ1, **Se-2** was induced to a face-on packing mode by PJ1, while **Se-1** retained its edge-on packing mode. Due to the ordered molecular packing and fiber interpenetrating morphology of the **Se-2**/PJ1 blend, the charge transport and extraction ability were improved. The improved morphology, together with its higher driving force, led to a suppressed energy transfer and more efficient charge generation. Consequently, an improved J_{sc} and FF were obtained in the device based on **Se-2**/PJ1. The probable face-on interfacial orientation in **Se-2**/PJ1 facilitated low V_{oc} loss, which is in conflict with its higher HOMO energy level (equal to higher driving force for hole transfer), resulting in the high V_{oc} and J_{sc} being concurrently obtained in the **Se-2**/PJ1 device. By comparison with other types of OSCs, we emphasize the importance of enhancing the Flory–Huggins interaction parameter in further photovoltaic material design in SM_D/P_A-type OSCs. Our results deepen the understanding of the morphology effect on the device performances, especially for the new type of SM_D/P_A OSCs, which would provide a useful guidance for high efficiency OSCs materials design.

Conflicts of interest

There are no conflicts to declare.

Acknowledgements

We are grateful for the financial support provided by the National Natural Science Foundation of China (51973044), and the Youth Innovation Promotion Association, Chinese Academy of Sciences.

References

1 Z.-G. Zhang, Y. Bai and Y. Li, *Chin. J. Polym. Sci.*, 2020, **39**, 1–13.
2 Z.-G. Zhang, Y. Yang, J. Yao, L. Xue, S. Chen, X. Li, W. Morrison, C. Yang and Y. Li, *Angew. Chem., Int. Ed.*, 2017, **56**, 13503–13507.
3 Z. G. Zhang and Y. Li, *Angew. Chem., Int. Ed.*, 2020, 4422–4433.
4 Q. Fan, W. Su, S. Chen, W. Kim, X. Chen, B. Lee, T. Liu, U. A. Méndez-Romero, R. Ma, T. Yang, W. Zhuang, Y. Li, Y. Li, T.-S. Kim, L. Hou, C. Yang, H. Yan, D. Yu and E. Wang, *Joule*, 2020, **4**, 658–672.
5 Z. Lin, L. Zhang, S. Tu, W. Wang and Q. Ling, *Sol. Energy*, 2020, **201**, 489–498.
6 Q. Fan, Q. An, Y. Lin, Y. Xia, Q. Li, M. Zhang, W. Su, W. Peng, C. Zhang, F. Liu, L. Hou, W. Zhu, D. Yu, M. Xiao, E. Moons, F. Zhang, T. D. Anthopoulos, O. Inganäs and E. Wang, *Energy Environ. Sci.*, 2020, **12**, 5017–5027.
7 G. Wang, F. S. Melkonyan, A. Facchetti and T. J. Marks, *Angew. Chem., Int. Ed.*, 2019, **58**, 4129–4142.
8 Q. Wu, W. Wang, T. Wang, R. Sun, J. Guo, Y. Wu, X. Jiao, C. J. Brabec, Y. Li and J. Min, *Sci. China: Chem.*, 2020, **63**, 1449.
9 Y. Xu, J. Yuan, S. Zhou, M. Seifrid, L. Ying, B. Li, F. Huang, G. C. Bazan and W. Ma, *Adv. Funct. Mater.*, 2019, **29**, 1806747.
10 A. Facchetti, *Mater. Today*, 2013, **16**, 123–132.
11 J. Du, K. Hu, J. Zhang, L. Meng, J. Yue, I. Angunawela, H. Yan, S. Qin, X. Kong, Z. Zhang, B. Guan, H. Ade and Y. Li, *Nat. Commun.*, 2021, **12**, 5264.
12 J. Du, K. Hu, L. Meng, I. Angunawela, J. Zhang, S. Qin, A. Liebman-Pelaez, C. Zhu, Z. Zhang, H. Ade and Y. Li, *Angew. Chem., Int. Ed.*, 2020, 15181–15185.
13 T. Jia, J. Zhang, W. Zhong, Y. Liang, K. Zhang, S. Dong, L. Ying, F. Liu, X. Wang, F. Huang and Y. Cao, *Nano Energy*, 2020, **72**, 104718.
14 W. Wang, Q. Wu, R. Sun, J. Guo, Y. Wu, M. Shi, W. Yang, H. Li and J. Min, *Joule*, 2020, **4**, 1070–1086.
15 R. Sun, W. Wang, H. Yu, Z. Chen, X. Xia, H. Shen, J. Guo, M. Shi, Y. Zheng, Y. Wu, W. Yang, T. Wang, Q. Wu, Y. Yang, X. Lu, J. Xia, C. J. Brabec, H. Yan, Y. Li and J. Min, *Joule*, 2021, **5**, 1548–1565.
16 Z. Zhang, J. Miao, Z. Ding, B. Kan, B. Lin, X. Wan, W. Ma, Y. Chen, X. Long, C. Dou, J. Zhang, J. Liu and L. Wang, *Nat. Commun.*, 2019, **10**, 3271.
17 J. Miao, B. Meng, Z. Ding, J. Liu and L. Wang, *J. Mater. Chem. A*, 2020, **8**, 10983–10988.
18 L. Zhu, Z. Tu, Y. Yi and Z. Wei, *J. Phys. Chem. Lett.*, 2019, **10**, 4888–4894.
19 R. Wang, C. Zhang, Q. Li, Z. Zhang, X. Wang and M. Xiao, *J. Am. Chem. Soc.*, 2020, **142**, 12751–12759.
20 F. Jin, J. Yuan, W. Guo, Y. Xu, Y. Zhang, C. Sheng, W. Ma and H. Zhao, *Adv. Funct. Mater.*, 2018, **28**, 1801611.
21 N. A. Ran, S. Roland, J. A. Love, V. Savikhin, C. J. Takacs, Y.-T. Fu, H. Li, V. Coropceanu, X. Liu, J.-L. Brédas, G. C. Bazan, M. F. Toney, D. Neher and T.-Q. Nguyen, *Nat. Commun.*, 2017, **8**, 79.
22 H. Kang, W. Lee, J. Oh, T. Kim, C. Lee and B. J. Kim, *Acc. Chem. Res.*, 2016, **49**, 2424–2434.
23 J. S. Park, N. Choi, C. Lee, S. Lee, J.-W. Ha, D.-H. Hwang and B. J. Kim, *Chem. Mater.*, 2020, **32**, 3585–3596.
24 J. Liu, J. Han, Q. Liang, J. Xin, Y. Tang, W. Ma, X. Yu and Y. Han, *ACS Omega*, 2018, **3**, 7603–7612.
25 C. Li, J. Zhou, J. Song, J. Xu, H. Zhang, X. Zhang, J. Guo, L. Zhu, D. Wei, G. Han, J. Min, Y. Zhang, Z. Xie, Y. Yi, H. Yan, F. Gao, F. Liu and Y. Sun, *Nat. Energy*, 2021, 605–613.
26 R. Zhou, Z. Jiang, Y. Shi, Q. Wu, C. Yang, J. Zhang, K. Lu and Z. Wei, *Adv. Funct. Mater.*, 2020, **30**, 2005426.

27 Q. Wu, D. Deng, R. Zhou, J. Zhang, W. Zou, L. Liu, S. Wu, K. Lu and Z. Wei, *ACS Appl. Mater. Interfaces*, 2020, **12**, 25100–25107.

28 D. Deng, Y. Zhang, L. Yuan, C. He, K. Lu and Z. Wei, *Adv. Energy Mater.*, 2014, **4**, 1400538.

29 D. Deng, Y. Zhang, J. Zhang, Z. Wang, L. Zhu, J. Fang, B. Xia, Z. Wang, K. Lu, W. Ma and Z. Wei, *Nat. Commun.*, 2016, **7**, 13740.

30 X. Zhang, D. Zhang, Q. Zhou, R. Wang, J. Zhou, J. Wang, H. Zhou and Y. Zhang, *Nano Energy*, 2019, **56**, 494–501.

31 F. D. Eisner, M. Azzouzi, Z. Fei, X. Hou, T. D. Anthopoulos, T. J. S. Dennis, M. Heeney and J. Nelson, *J. Am. Chem. Soc.*, 2019, **141**, 6362–6374.

32 Y. Xie, W. Huang, Q. Liang, J. Zhu, Z. Cong, F. Lin, S. Yi, G. Luo, T. Yang, S. Liu, Z. He, Y. Liang, X. Zhan, C. Gao, H. Wu and Y. Cao, *ACS Energy Lett.*, 2019, **4**, 8–16.

33 J. T. Bloking, T. Giovenzana, A. T. Higgs, A. J. Ponec, E. T. Hoke, K. Vandewal, S. Ko, Z. Bao, A. Sellinger and M. D. McGehee, *Adv. Energy Mater.*, 2014, **4**, 1301426.

34 M. A. Adil, J. Zhang, D. Deng, Z. Wang, Y. Yang, Q. Wu and Z. Wei, *ACS Appl. Mater. Interfaces*, 2018, **10**, 31526–31534.